Tissue Damage Control Algorithm for Hyperthermia Based Cancer Treatments

Gustavo Resende Fatigate[2][0000−0002−2600−2974], Rafael Felipe Coelho Neves[3][0000−0003−3819−1714], Marcelo Lobosco[1,2⋆][0000−0002−7205−9509], and Ruy Freitas Reis[1][0000−0001−5215−3744]

[1] Departamento de Ciência da Computação, Universidade Federal de Juiz de Fora, Brazil
[2] Pós-Graduação em Modelagem Computacional, Universidade Federal de Juiz de Fora, Brazil
[3] Instituto Federal de Educação, Ciência e Tecnologia do Sul de Minas Gerais, Poços de Caldas, Brazil
marcelo.lobosco@ice.ufjf.br

Abstract. Cancer is a worldwide health problem. The fatality rate of some types of cancer motivates the scientific community to improve the standard techniques used to fight against this disease, as well as to investigate new forms of treatments. One of these emerging treatments is hyperthermia using the injection of magnetic nanoparticles into the tumour area. Its basic idea is to heat the target tumour tissue leading to its necrosis. This study simulates the bioheat processes using Pennes' model to evaluate the tissue damage *in silico*. Furthermore, the differential evolution optimisation technique is applied to suggest the optimal location of injection considering the minimisation of damage to the healthy tissue and the maximisation of the tumour necrosis. The results suggest that the proposed algorithm is a promising tool for aiding hyperthermia-based treatment planning.

Keywords: Hyperthermia · Cancer · Bioheat · Optimization · Differential Evolution.

1 Introduction

According to the World Health Organisation (WHO), cancer is the second biggest cause of death worldwide, and it is estimated that around 9.6 million people died in 2018 due to this disease [28]. Nearly 70% of the cancer cases occurs in low or middle-income countries. Furthermore, 30% of the deaths could be avoid with the early diagnosis and proper treatment [16].

Due to its high mortality rates, cancer is a public health concern worldwide, which motivates the scientific community to study and develop new strategies to fight against this disease. Among the methods to treat cancer patients, in this study we highlight hyperthermia which works as an adjuvant technique to

---
⋆ corresponding author

help existing treatments such as radiotherapy and chemotherapy. Recent studies show that hyperthermia is also presenting relevant results when combined with innovative clinical options such as hadron therapy for treating pancreatic cancer [4].

Hyperthermia procedure consists in overheating the tumour tissue over 43^oC degrees leading the tissue to necrosis [21]. The necrosis is obtained through the injection of nanoparticles into the tumour tissue. The nanoparticles produce heat through Brownian and Neelian relaxation when submitted to a magnetic field using low frequency [14]. This treatment has the advantage of being semi-invasive once it can reach the tumour intravenously or through direct injection.

The Pennes model [17] is commonly used to describe the heat transfer in living tissue, presenting similarities between the theoretical and experimental results [15, 21, 23, 27]. A large number of works use this model in order to study the bioheat [6–8, 23]. Moreover, the original Pennes model can be modified to include the hyperthermia cancer treatment process [2, 13, 18, 25, 26].

This study uses differential evolution (DE) to search for the best position for the injection of the magnetic nanoparticles to maximise the death of the tumour tissue and to minimise the healthy tissue affected by the hyperthermia process. DE is a heuristic-based algorithm used to find a set of parameters that minimise a known function [3, 12, 19, 20]. Furthermore, DE is already applied in correlated studies of hyperthermia to optimise the value of radio frequency power, amplitude and/or phase [5, 9, 29]. The heat distribution is evaluated using the Pennes bioheat model through partial differential equations (PDE) via the finite difference method (FDM). To evaluate the objective function in DE we use the bioheat model to obtain the temperature distribution of the modelled tissue after 50 minutes of hyperthermia treatment. This information is used to measure the amount of healthy and tumour tissues influenced by the process.

We organise this paper as follows. Section 2 describes the bioheat model, numerical approximation and the optimisation strategy. The results are presented in section 3 and discussed in section 4. Finally, section 5 presents the conclusions and plans for future work.

2   Methods

2.1   Mathematical Model

The choice of the Pennes model is due to its simplicity, reducing the computational cost of simulations. So, including the hyperthermia heat source the model is expressed as follows:

$$\begin{cases} \rho c \dfrac{\partial T}{\partial t} = \nabla \cdot k\nabla T + \omega_b \rho_b c_b (T_a + T) + Q_m + Q_r & \text{in } \Omega \times I \\ k\nabla T \cdot \vec{n} = 0 & \text{in } \partial\Omega \times I \\ T(\cdot, 0) = T_0 & \text{in } \Omega, \end{cases} \quad (1)$$

where $\Omega \subset \mathbb{R}^2$ is the equation spatial domain, $I \subset \mathbb{R}^+$ is the time domain, $T : \Omega \times I \to \mathbb{R}^+$ is the tissue temperature field; ρ, c and k are density, specific heat

and thermal conductivity of the tissue, respectively; ρ_b, c_b and ω_b are density, specific heat of the blood and blood perfusion, respectively; T_a and T_0 are the blood temperature and the initial temperature, respectively; Q_m and Q_r are the metabolic heat source and the heat generated by the hyperthermia treatment, respectively.

It is important to emphasise the simplifications made by Pennes in the proposition of his model. The heat exchanges between blood and the tissue occur between capillaries and arterioles. The blood flow is assumed to be isotropic, $i.e.$ there is no directional preference. The vascular geometry was disregarded, and the blood reaches the arterioles at a body temperature, in our case 37^oC [10].

The heat generated by the hyperthermia treatment (Q_r) is calculated by the specific absorption rate (SAR) through the Equation (2) [22]. This equation models the heat generated considering a set of injections used in the hyperthermia process. In this study it was approximated by the following equation:

$$Q_r = \sum_{i=1}^{N_p} A e^{-r(\vec{x})_i^2/r_{0,i}^2},\qquad(2)$$

where N_p is the number of injections points in the tissue; A is the energy maximum strength of the volumetric heat generation rate, $r(\vec{x})_i^2$ is the Euclidean distance to the injection point, $i.e.$ $r = ||\vec{x} - \vec{x_0}||_2$; x_0 is the injection position; r_0 is the radius of coverage of hyperthermia.

2.2 Numerical Scheme

The numerical method used to solve Equation (1) is the Finite Difference Method (FDM), considering a heterogeneous medium. We consider the closed domain Ω discretised into a set of regular points defined by $S_s = \{(x_i, y_j); i = 0, 1, \cdots, N_x; j = 0, 1, \cdots, N_y\}$, where N_x and N_y are the number of intervals of length $h_x = h_y = h$. Moreover, the time discretisation of the time domain I is partitioned into N_t equal time intervals of length h_t, $i.e.$ $S_t = \{(t_n); n = 0, 1, \cdots, N_t\}$. To obtain the discrete form of the model, we employ an FTCS (Forward-Time Central-Space), resulting in an explicit numerical method. This scheme has convergence order $O(h^2, h_t)$ [11].

$$T_{i,j}^{n+1} = \frac{h_t}{\rho c}\left[\frac{k_{i+1/2,j}(T_{i+1,j}^n - T_{i,j}^n) - k_{i-1/2,j}(T_{i,j}^n - T_{i-1,j}^n)}{h^2}\right.$$
$$+ \frac{k_{i,j+1/2}(T_{i,j+1}^n - T_{i,j}^n) - k_{i,j-1/2}(T_{i,j}^n - T_{i,j-1}^n)}{h^2}\qquad(3)$$
$$\left. + \rho_b c_b \omega_b \left(T_a - T_{i,j}^n\right) + Q_m + Q_r\right] + T_{i,j}^n.$$

2.3 Differential evolution

Differential evolution (DE) is a stochastic-heuristic algorithm for global optimisation [24]. DE is based on natural evolution, presenting generations, selections, mutations and the capacity of an individual to survive the environment [1].

As an evolutionary algorithm, DE works in generations and presents a population with a fixed number of individuals. Given an initial population, the next generation (or offspring) is formed considering mutation and the crossing between the individuals of the same generation. This process continues until it achieves the convergence of results or the maximum number of generations.

To maximise the damage to the tumour tissue and to minimise the damage to the healthy tissue, we employed the following minimisation problem:

$$\min O(p) = 300 - N_t - (100 - N_h) - 100\beta, \tag{4}$$

where p is the set of points to be estimated. $N_t \in [0, 100]$ is the percentage of tumour tissue necrosis and $N_h \in [0, 100]$ is the percentage of healthy tissue necrosis. $\beta \in \{0, 1\}$ is a variable that assumes 1 when entire tumour reaches 43^oC or more and 0 otherwise.

We consider the mutation strategy *best/1/bin*, *i.e.* the best individual (X_{best}) and two more random individuals are chosen (X_a and X_b). The random individuals are subtracted and multiplied by the mutation factor F. The result is added to X_{best}, originating the mutation vector X_p as shown in Eq (5):

$$X_p^{i+1} = X_{best}^i + F * (X_a^i - X_b^i). \tag{5}$$

The next step is the crossover operation applied to individuals of the same generation. This operation considers the mutation vector and a target vector, randomly chosen from the population. A new vector of individuals is created and its content depends on a random number generated for each position of the vector. If the number is smaller than the crossing constant C, the value is taken from the mutation vector, otherwise, the value is taken from the target vector, *i.e*:

$$U^{i+1} = \begin{cases} X_p^{i+1}, & \text{if } r_i \leq C \\ X_r^i, & \text{otherwise.} \end{cases} \tag{6}$$

Finally, the fitness of the trial vector is calculated considering the objective function and compared with the target vector. The individuals with smaller fitness are considered to pass to the next generation.

3   Results

All results were obtained using of Google Colab platform and C/C++ programming language.

We consider a two-dimensional squared domain of lengths equal to $0.1m$ representing the simulated tissue and circular tumours with radii equal to $0.01m$. We perform three scenarios: 1) one tumour and one injection point (see Figure 1A), 2) two tumours and two injections points (see Figure 2A), and 3) three tumours and three injections points (see Figure 3A). All tumours were randomly positioned in the mesh. The simulated domain is represented in Figures 1-3 A.

Besides, Equation (1) is solved using the parameters described in Tables 1 and 2, and the initial condition $T_0 = 37.0$ is used for all performed simulations.

Table 1. Parameters used to solve Equation (1) for both tumour and healthy tissues.

Parameters	Unit	Healthy Tissue	Tumour Tissue
k	W/m^oC	0.51	0.64
ω_b	s^{-1}	5.0×10^{-4}	1.25×10^{-3}
ρ	Kg/m^3	1000.0	1000.0
ρ_b	Kg/m^3	1000.0	1000.0
Q_m	W/m^3	420.0	4200.0
c	J/Kg^oC	4200.0	4200.0
c_b	J/Kg^oC	4200.0	4200.0

Table 2. Parameters used in the hypertermia treatment (see Equation (2)).

Parameters	Unit	Value
N_p	$-$	3
A	W	0.05×10^6
r_0	m	1.9×10^{-2}

For each scenario, the optimisation process was performed 10 times, considering different seeds to ensure that the algorithm does not converge to a local minimum. Figures 4, 5 and 6 present a boxplot of all performed simulation results, considering one, two and three tumours, respectively. It is important to note that all points presented a standard deviation of the order of 10^{-3}.

Figures 1C, 2C and 3C show the simulation of the hyperthermia process considering the best result obtained by the optimisation process. Moreover, in all three scenarios, we perform a naive tentative considering the injection point in the centre of the tumour, which is illustrated by Figures 1B, 2B and 3B. These results represents the temperature distribution of the tissue after 50 minutes of treatment. The black solid line delimits the entire part of the tissue that reached 43^oC or more, *i.e.* the region of the tissue that suffered necrosis, and the black dots represents the injection points.

In the first scenario, we consider a tumour centred at $(0.050, 0.050)$ (Figure 1A). Figure 1C presents the result of the optimisation, and the best position found is in the centre of the tumour, *i.e.* the same as the naive approach (Figure 1B).

Figure 2 shows the results of the second scenario, *i.e.* the tissue with two tumours centred at $(0.050, 0.030)$ and $(0.050, 0.060)$, respectively. In this case, the optimisation result is different from the naive tentative: the amount of healthy
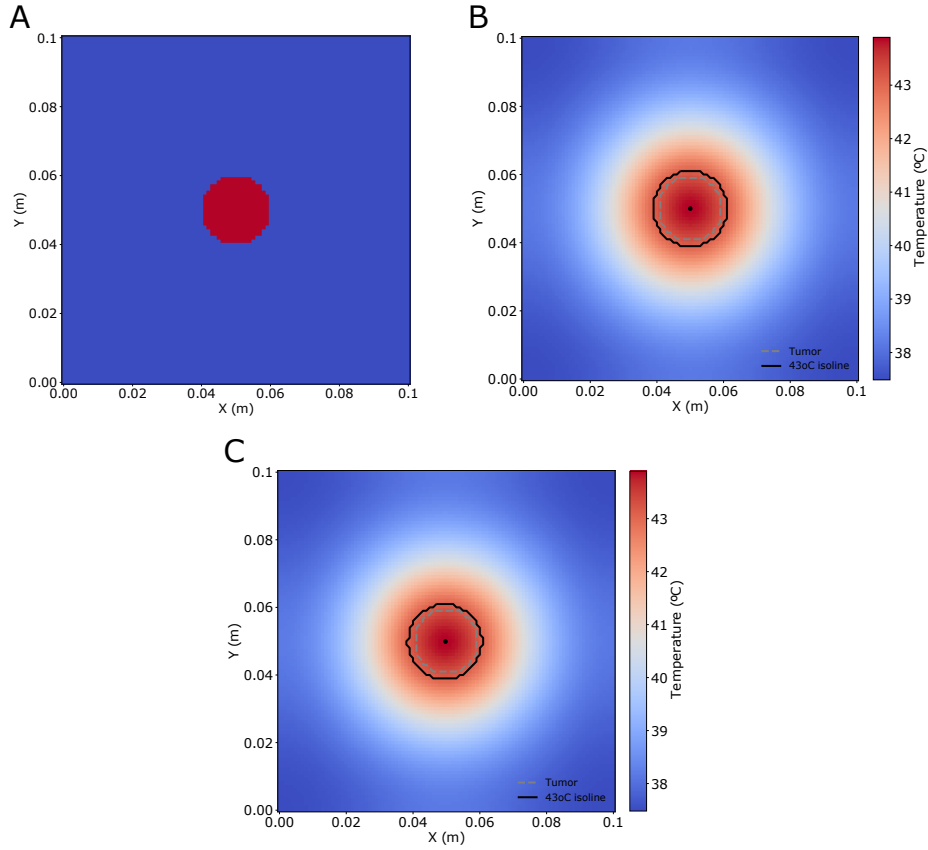
A

B

C

Fig. 1. The simulated tissue and the results for the first scenario. In Panel A the red area represents the tumour tissue, and the blue area the healthy tissue. The tumour has a radius of $0.01m$, and its centre is positioned at $(0.050, 0.050)$. Panels B and C present the results of the numerical solution of Equation (1) at $t = 50$min. In Panel B, the simulation considers $P_1 = (0.050, 0.050)$, *i.e.* the centre of the tumour. In Panel C, the optimisation processes found $P_1 = (0.0498984, 0.0497171)$. The black dots represent the position of P_1, the solid black contour highlights the portion of the domain that reaches $T \geq 43^o$, and the dashed grey contour indicates the tumour location.

tissue affected by the treatment is reduced from 16.51% (Figure 2 B) to 15.18% (Figure 2 C). In other words, the optimisation reduced the damage to the healthy tissue.

Finally, the third scenario was performed in the tissue with three tumours (Figure 3A). In this case, the first tumour has its centre located at $(0.035, 0.025)$, the second tumour at $(0.065, 0.050)$, and the third tumour at $(0.035, 0.075)$. In the third scenario, the optimised solution is different from the naive tentative, similarly to the observed in the second scenario. In this case, the naive tentative
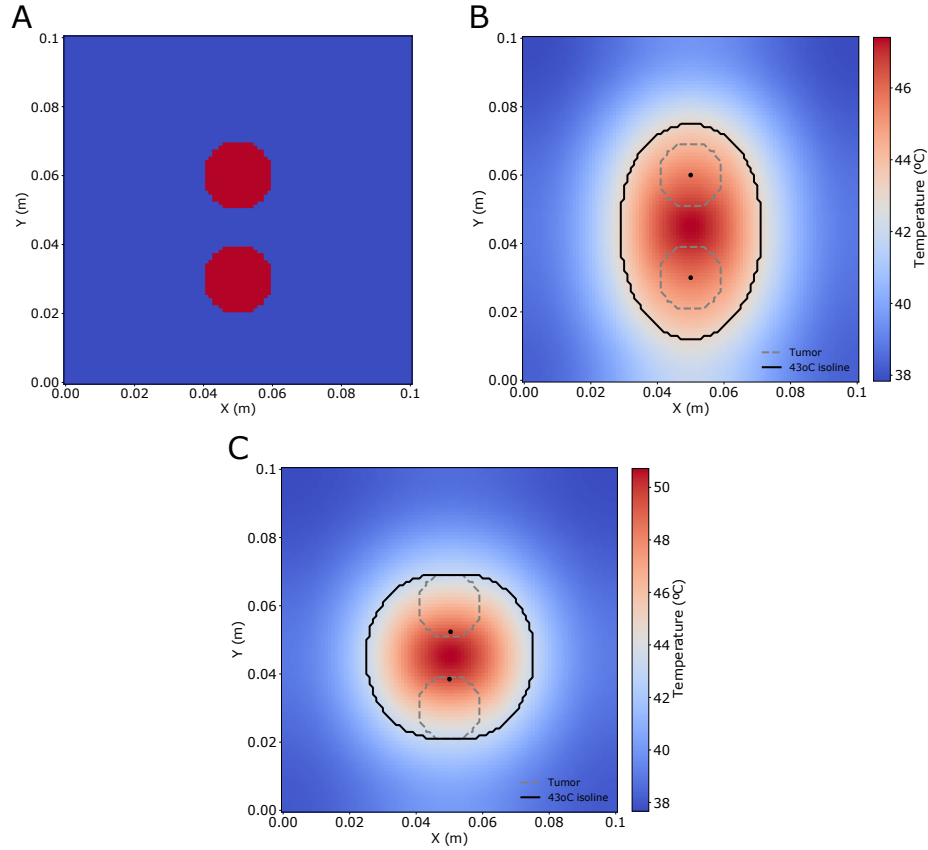
A

B

C

Fig. 2. The simulated tissue and the results for the second scenario. In Panel A, the red area represents the tumour tissue, and the blue area the healthy tissue. The tumours have a radius of $0.01m$ each and their centres are positioned at $(0.050, 0.030)$, and $(0.050, 0.060)$, respectively. Panels B and C present the results of the numerical solution of Equation (1) at $t = 50$min. In Panel B, the simulation considers $P_1 = (0.050, 0.030)$, and $P_2 = (0.050, 0.060)$, *i.e.* the centre of each tumour. In Panel C, the optimisation processes found $P_1 = (0.0500118, 0.0384764)$, and $P_2 = (0.0503467, 0.0523711)$. The black dots represent the position of P_1 and P_2, the solid black contour highlights the portion of the domain that reaches $T \geq 43^o$, and the dashed grey contour indicates the tumour location.

result in 40% of healthy tissue necrosis while the optimised one affects only about 30% of the healthy tissue.

4   Discussion

Figure 4, 5 and 6 show a boxplot for 10 executions of the optimisation process. All executions succeed in obtaining the necrosis of the entire tumour tissue,
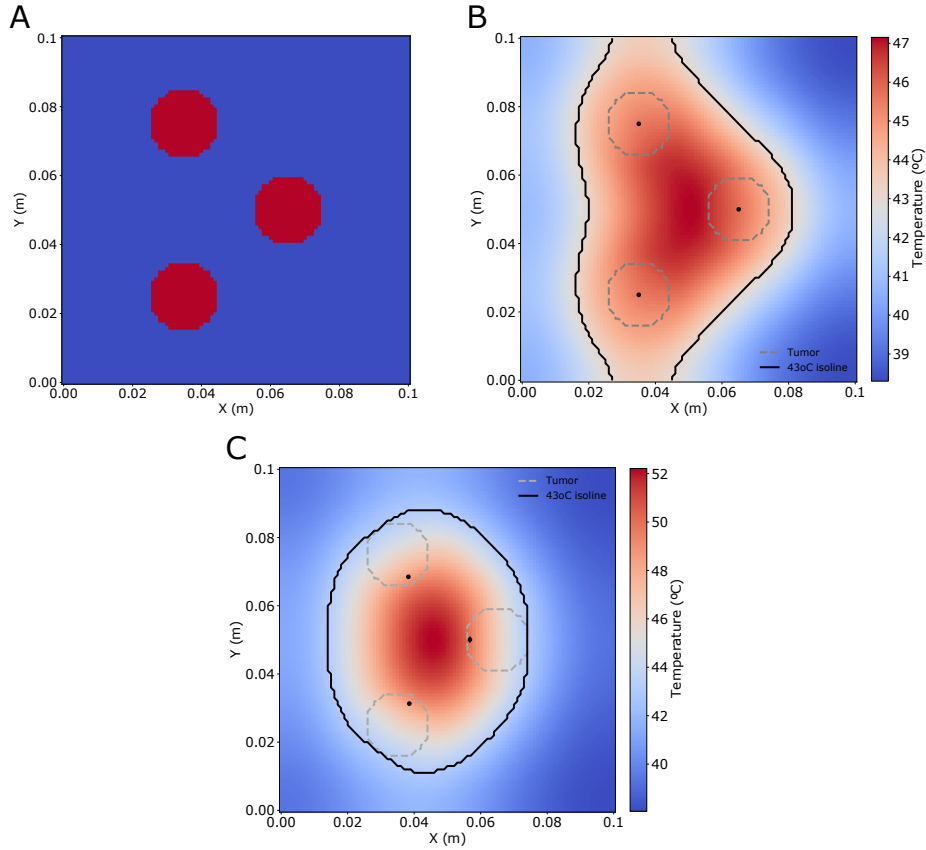
Fig. 3. The simulated tissue and the results for the third scenario. In Panel A, the red area denotes the tumour tissue, and the blue area the healthy tissue. The tumours have a radius of $0.01m$ each and their centres are positioned at $(0.035, 0.025)$, $(0.065, 0.050)$ and $(0.035, 0.075)$. Panels B and C present the results for numerical solution of Equation (1) at $t = 50$min. In Panel B, the simulation considers $P_1 = (0.035, 0.025)$, $P_2 = (0.065, 0.050)$, and $P_3 = (0.035, 0.075)$, *i.e.* the centre of each tumour. In Panel C, the optimisation processes found $P_1 = (0.0313107, 0.0614578)$, $P_2 = (0.0500641, 0.0432409)$, and $P_3 = (0.0684779, 0.0617488)$. The black dots represent the position of P_1, P_2 and P_3, the solid black contour highlights the portion of the domain that reaches $T \geq 43^o$, and the dashed grey contour indicates the tumour location.

suggesting that the proposed scheme offers a robust algorithm for hyperthermia-based cancer treatments. Moreover, Figure 4, 5 and 6 show that even considering multiple executions of the proposed scheme, the solution converges for a similar result. Moreover, the results present a standard deviation smaller than 2%.

Furthermore, the proposed strategy proved to be useful, once the optimisation process results in a non-trivial solution that minimises tissue damage. For
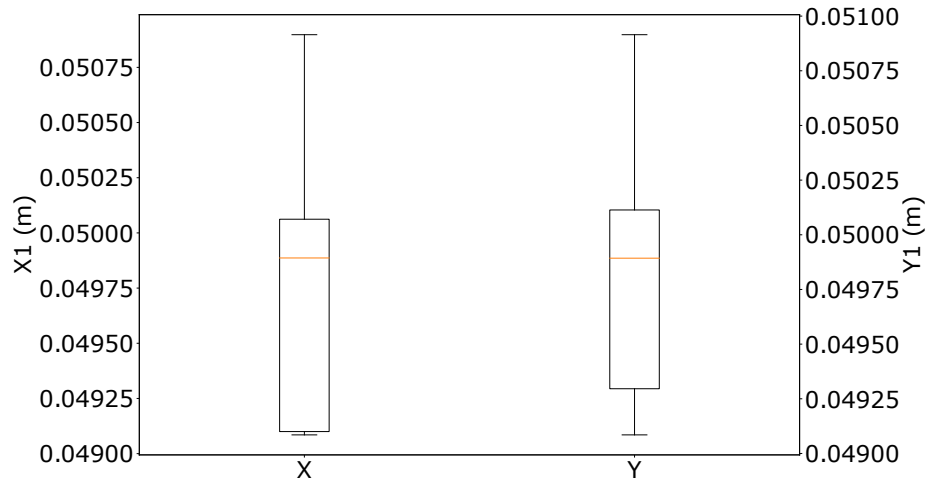
Fig. 4. Boxplot for the optimised P_1 position. The left axis represents the x coordinate of P_1, while the right axis represents the y coordinate.
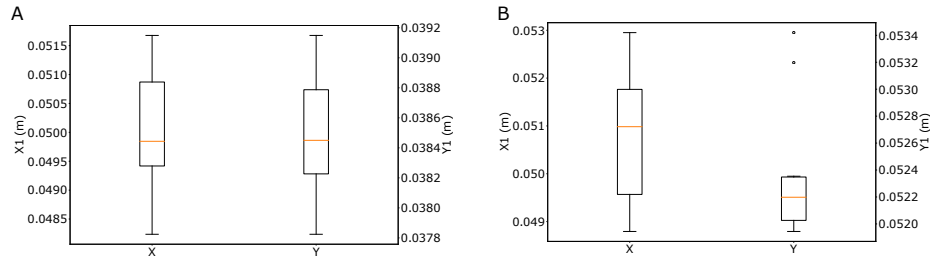

Fig. 5. Panels A and B show the boxplots for the optimised P_1 and P_2 positions, respectively, considering all the ten tests. The left axis represents the x coordinate of the point, while the right axis represents the y coordinate.

example, Figure 3 B demonstrate that the trivial guess does succeed in destroying the tumour, but produces higher damage to the healthy tissue. The proposed strategy succeeds in causing less damage to the healthy tissue by formulating a minimisation problem that penalises damage to healthy tissue and rewards total tumour destruction. It is worthwhile to notice that none of the injection points has direct contact with the tumours. A possible explanation is that cancerous tissues have higher values of thermal conductivity, blood perfusion and metabolic heat.

5   Conclusions and Future Works

This work presents a tool for aiding hyperthermia-based treatment planning. The proposed algorithm suggests that it is possible to find optimal locations for
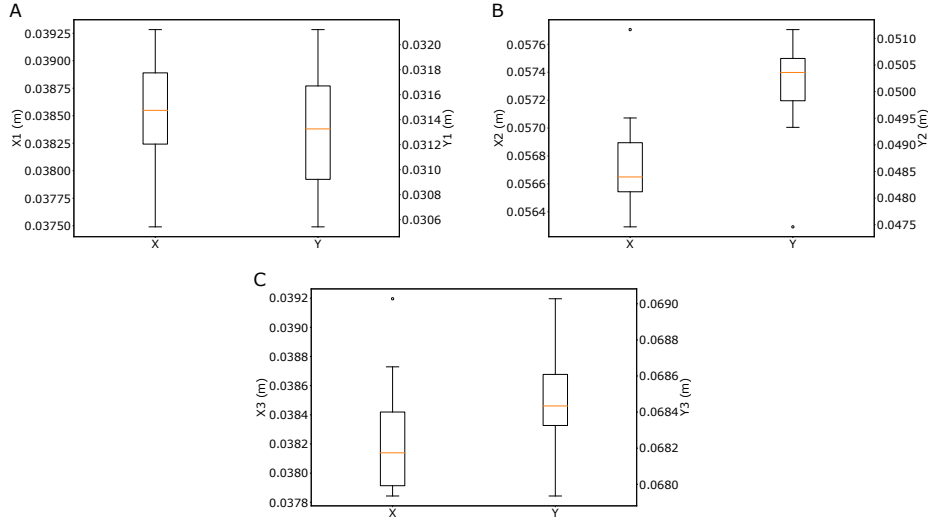
Fig. 6. Panels A, B and C show the boxplots for the optimised P_1, P_2 and P_3 positions, respectively, considering all the ten tests. The left axis represents the x coordinate of the point, while the right axis represents the y coordinate.

injecting the nanoparticles and for inducing the heat on hyperthermia treatment considering both damages of the entire tumour and minimal damage to healthy tissue. Moreover, this study also indicates that the optimal position for injecting the nanoparticles might be in a non-trivial location such as in the healthy tissue near the target area instead of injecting inside the tumour site.

For future works, we are planning to expand the simulation to a more realistic tissue, considering a three-dimensional domain as well as patient-based tumour formats. Moreover, a parallel strategy is necessary, once the average time for obtaining each optimised site is $2h31m$. So, the reduction of computational time is going to be even more relevant when considering the three-dimensional model.

Acknowledgments

References

1. Amasifen, J.C.C., Romero, R., Mantovani, J.R.: Algoritmos evolutivos dedicados à reconfiguração de redes radiais de distribuição sob demandas fixas e variáveis: estudo dos operadores genéticos e parâmetros de controle. Sba: Controle & Automação Sociedade Brasileira de Automatica **16**(3), 303–317 (2005)

2. Attar, M.M., Haghpanahi, M., Amanpour, S., Mohaqeq, M.: Analysis of bioheat transfer equation for hyperthermia cancer treatment. Journal of Mechanical Science and Technology **28**(2), 763–771 (2014)

3. Babu, B., Jehan, M.M.L.: Differential evolution for multi-objective optimization. In: The 2003 Congress on Evolutionary Computation, 2003. CEC'03. vol. 4, pp. 2696–2703. IEEE (2003)

4. Brero, F., Albino, M., Antoccia, A., Arosio, P., Avolio, M., Berardinelli, F., Bettega, D., Calzolari, P., Ciocca, M., Corti, M., et al.: Hadron therapy, magnetic nanoparticles and hyperthermia: A promising combined tool for pancreatic cancer treatment. Nanomaterials **10**(10), 1919 (2020)

5. Cappiello, G., McGinley, B., Elahi, M.A., Drizdal, T., Paulides, M.M., Glavin, M., O'Halloran, M., Jones, E.: Differential evolution optimization of the sar distribution for head and neck hyperthermia. IEEE Transactions on Biomedical Engineering **64**(8), 1875–1885 (2016)

6. Charny, C.K.: Mathematical models of bioheat transfer. In: Advances in heat transfer, vol. 22, pp. 19–155. Elsevier (1992)

7. Ezzat, M.A., AlSowayan, N.S., Al-Muhiameed, Z.I., Ezzat, S.M.: Fractional modelling of pennes' bioheat transfer equation. Heat and Mass Transfer **50**(7), 907–914 (2014)

8. Ferrás, L.L., Ford, N.J., Morgado, M.L., Nóbrega, J.M., Rebelo, M.S.: Fractional pennes' bioheat equation: theoretical and numerical studies. Fractional Calculus and Applied Analysis **18**(4), 1080–1106 (2015)

9. Gas, P., Miaskowski, A.: Sar optimization for multi-dipole antenna array with regard to local hyperthermia. Przeglad Elektrotechniczny **1**(95), 17–20 (2019)

10. Jiji, L.M.: Heat Conduction. Springer-Verlag Berlin Heidelberg (2009)

11. LeVeque, R.J.: Finite difference methods for ordinary and partial differential equations: steady-state and time-dependent problems. SIAM (2007)

12. Liu, R., Fan, J., Jiao, L.: Integration of improved predictive model and adaptive differential evolution based dynamic multi-objective evolutionary optimization algorithm. Applied Intelligence **43**(1), 192–207 (2015)

13. Miaskowski, A., Sawicki, B.: Magnetic fluid hyperthermia modeling based on phantom measurements and realistic breast model. IEEE transactions on biomedical engineering **60**(7), 1806–1813 (2013)

14. Moros, E.: Physics of thermal therapy: fundamentals and clinical applications. CRC Press (2012)

15. Ng, E.Y.K., Kumar, S.D., et al.: Physical mechanism and modeling of heat generation and transfer in magnetic fluid hyperthermia through néelian and brownian relaxation: a review. Biomedical engineering online **16**(1), 1–22 (2017)

16. OPAS/OMS: Organização mundial da saúde. Published Electronically - https://www.paho.org/pt/topicos/cancer. Last acessed 02 Feb 2022 (2022)

17. Pennes, H.H.: Analysis of tissue and arterial blood temperature in the restind human forearm. Journal of Applied Phisiology **1**, 93–122 (1948)

18. Reis, R.F., dos Santos Loureiro, F., Lobosco, M.: A parallel 2d numerical simulation of tumor cells necrosis by local hyperthermia. Journal of Physics: Conference Series **490**(012138) (2014)

19. Rogalsky, T., Kocabiyik, S., Derksen, R.: Differential evolution in aerodynamic optimization. Canadian Aeronautics and Space Journal **46**(4), 183–190 (2000)

20. Ronkkonen, J., Kukkonen, S., Price, K.V.: Real-parameter optimization with differential evolution. In: 2005 IEEE congress on evolutionary computation. vol. 1, pp. 506–513. IEEE (2005)

21. Salloum, M., Ma, R., Zhu, L.: Enhancement in treatment planning for magnetic nanoparticle hyperthermia: Optimization of the heat absorption pattern. International Journal of Hyperthermia **25**(4), 309–321 (2009)
22. Salloum, M., Ma, R., Zhu, L.: An in-vivo experimental study of temperature elevations in animal tissue during magnetic nanoparticle hyperthermia. International Journal of Hyperthermia **24**(7), 589–601 (2008)
23. Shih, T.C., Yuan, P., Lin, W.L., Kou, H.S.: Analytical analysis of the pennes bioheat transfer equation with sinusoidal heat flux condition on skin surface. Medical Engineering & Physics **29**(9), 946–953 (2007)
24. Storn, R., Price, K.: Differential evolution–a simple and efficient heuristic for global optimization over continuous spaces. Journal of global optimization **11**(4), 341–359 (1997)
25. Suleman, M., Riaz, S.: 3d in silico study of magnetic fluid hyperthermia of breast tumor using fe3o4 magnetic nanoparticles. Journal of thermal biology **91**, 102635 (2020)
26. Tucci, C., Trujillo, M., Berjano, E., Iasiello, M., Andreozzi, A., Vanoli, G.P.: Pennes' bioheat equation vs. porous media approach in computer modeling of radiofrequency tumor ablation. Scientific Reports **11**(1), 1–13 (2021)
27. Valente, A., Peters, F.C., de Souza, R.V.M., Mansur, W.J.: 3d numerical simulation of real-time temperature field in a hyperthermia cancer treatment using octree meshes. Journal of the Brazilian Society of Mechanical Sciences and Engineering **43**(1), 1–11 (2021)
28. WHO: World health organization. http://www.who.int/. Last acessed 20 Dec 2021 (2021)
29. Xu, L., Wang, X.: Comparison of two optimization algorithms for focused microwave breast cancer hyperthermia. In: 2018 International Applied Computational Electromagnetics Society Symposium-China (ACES). pp. 1–2. IEEE (2018)